

https://dspace.org/

CARRSSPipeline Flux Calibration and Nonlinear Reprojection for SALTRSS MultiObject Spectroscopy over 35009500s

George V. Kharchilava; Eric Gawiser; Matthew Hilton; Elizabeth Turner; Nicole M. Firestone ...

UNIV CHICAGO PRESS
https://hdl.handle.net/10539/47303
WOS

Downloaded from a DSpace repository. https://dspace.org/

Publications of the Astronomical Society of the Pacific, 137:034503 (11pp), 2025 March https://doi.org/10.1088/1538-3873/adb454
© 2025. The Author(s). Published by IOP Publishing Ltd on behalf of the Astronomical Society of the Pacific (ASP).

OPEN ACCESS

CARRSSPipeline: Flux Calibration and Nonlinear Reprojection for SALT-RSS Multi-Object Spectroscopy over 3500–9500 Å

George V. Kharchilava[1], Eric Gawiser[1,2], Matt Hilton[3], Elisabeth Turner[4], Nicole M. Firestone[1], and Kyoung-Soo Lee[5]
[1] Department of Physics and Astronomy, Rutgers, The State University of New Jersey, Piscataway, NJ 08854, USA
[2] School of Natural Sciences, Institute for Advanced Study, Princeton, NJ 08540, USA
[3] Wits Centre for Astrophysics, University of the Witwatersrand, Johannesburg, Braamfontein, Johannesburg, 2000, South Africa
[4] Department of Physics and Astronomy, Tufts University, Medford, MA 02155, USA
[5] Department of Physics and Astronomy, Purdue University, West Lafayette, IN 47907, USA
Received 2024 September 19; revised 2025 January 27; accepted 2025 February 6; published 2025 March 17

Abstract

The Robert Stobie Spectrograph (RSS) on the Southern African Large Telescope (SALT) offers multi-object spectroscopy over an 8′ field-of-view at resolutions up to $R \sim 3000$. Reduction is typically conducted using `RSSMOSPipeline`, which performs basic data calibrations, sky subtraction, and wavelength calibration. However, flux calibration of SALT-RSS using spectrophotometric standard star observations is difficult due to variable primary mirror illumination. We describe a novel approach where stars with Sloan Digital Sky Survey spectra are included as alignment stars on RSS slitmasks and then used to perform a rough flux calibration of the resulting data. RSS offers multiple settings that can be pieced together to cover the entire optical range, utilizing grating angle dithers to fill chip gaps. We introduce a nonlinear reprojection routine that defines an exponential wavelength array spanning 3500–9500 Å with gradually decreasing resolution and then reprojects several individual settings into a single 2D spectrum for each object. Our flux calibration and nonlinear reprojection routines are released as part of the Calibration And Reprojection for RSS Pipeline (`CARRSSPipeline`), that enables the extraction of full-optical-coverage, flux-calibrated, medium-resolution one-dimensional spectra.

Unified Astronomy Thesaurus concepts: Spectroscopy (1558); Galaxy spectroscopy (2171); Emission line galaxies (459); Astronomy data reduction (1861); Flux calibration (544)

1. Introduction

Nebular emission science involves the identification and investigation of emission lines and their fluxes, line ratios, and observed wavelengths. These can be used to determine the physical properties of the galaxies they originate from, including electron densities, ionization parameters, velocity dispersion, dust reddening, metallicities, and star formation rates. Studied holistically, these properties can reveal how the galaxies evolved through cosmic time. In order to accurately determine these characteristics, proper reduction must be carried out on observed spectroscopic data to remove or correct for both instrument systematics and external factors. Wavelength and flux calibration in particular are needed, with the latter posing challenges due to instrument limitations (see Section 4.1). Analyses of velocity dispersion and metallicity can be carried out prior to flux calibration and dust correction since these only require measurements of line widths or flux ratios of lines that are close to each other. However, accurate fluxes are required for flux ratios of well-separated lines, as well as determining other characteristics such as star formation rates. The Multi-Object Spectroscopy (MOS) mode on the Robert Stobie Spectrograph (RSS) on the Southern African Large Telescope (SALT) offers full optical wavelength coverage across several gratings, as well as resolutions of up to $R \sim 3000$ over an 8′ field-of-view. This allows us to resolve the roughly 2.7 Å separated [O II] doublets, and measure each central wavelength and line flux of [O II]λ3726 and [O II] λ3729.

There are several spectroscopic reduction pipelines made in Python[6] that are available for astronomers to use, such as `PyReduce`[7] (Piskunov et al. 2021), `PyDIS`[8], `specreduce`[9], and `Pypelt`[10] (Prochaska et al. 2020a, 2020b). However, some of these packages are only available for longslit spectroscopy while others only perform up to wavelength calibration. Even the versatile `Pypelt`, which does perform

Original content from this work may be used under the terms of the Creative Commons Attribution 3.0 licence. Any further distribution of this work must maintain attribution to the author(s) and the title of the work, journal citation and DOI.

[6] https://www.python.org/
[7] https://pyreduce-astro.readthedocs.io/en/latest/index.html
[8] https://github.com/StellarCartography/pydis
[9] https://github.com/astropy/specreduce
[10] https://pypeit.readthedocs.io/en/release/

flux calibration, does not include an RSS instrument package. That is why we seek to develop a pipeline using Python routines to carry out full data calibration, called the Calibration And Reprojection for the RSS Pipeline (CARRSSPipeline[11]). Our goal with this pipeline is to perform rough flux calibration on SALT-RSS MOS spectra to within 20% accuracy. This would allow us to measure ionization parameters using [O III]/[O II], dust reddening using Hα/Hβ, and metallicity determined from multiple indicators. These calibrations pose challenges due to the nature of both the instrumentation being used and the condition of the observations as discussed in Section 2, and we pick relatively high flux targets for our masks as priority objects together with dim filler targets, and alignment stars. Section 3 introduces the first steps in the reduction process, which are done by a preceding Python pipeline. We describe data handling and reduction processes of the CARRSSPipeline in Section 4, including the results of our novel approach to flux calibration and its statistics. Future directions and further developments are mentioned in Section 5.

2. Observations

Once SALT-RSS MOS data is collected and downloaded, it is subject to two pipelines to carry out all reduction steps: RSSMOSPipeline[12] (see Section 3) which performs flat-field correction, cosmic ray rejection, sky subtraction, and wavelength calibration, and our CARRSSPipeline (see Section 4) which performs flux calibration, sky subtraction correction, wavelength reprojection, continuum comparison, and line inspection. These pipelines are designed specifically to handle SALT-RSS MOS data. The second pipeline directly follows the first and outputs both 2D and 1D flux-calibrated, fully reprojected spectra.

Our mask labeled COSMOS-mask-B was created using the PySALT[13] (Crawford et al. 2010) user package for the SALT telescope, and observed during the 2021-2 semester as program 2021-2-SCI-026 (Principal Investigator Elisabeth Turner). The mask included emission-line targets at redshift $z < 0.4$ from the Hobby–Eberly Telescope Dark Energy Experiment survey (HETDEX: Ramsey et al. 1998; Gebhardt et al. 2021; Hill et al. 2021). Though [O II] is most commonly seen in our setting using the PG3000 grating, Figure 1 shows a PG2300 setting for COSMOS-mask-B with an [O II] doublet, as well as an [O III] doublet and Hβ emission. We also identify targets with Hα and [N II] lines in PG0900 for the same mask. In this paper, we follow one of these targets, called HETDEX J100041.45 +021331.8, throughout the reduction process, with the purpose of demonstrating accurate calibrations as well as maintaining the resolution of the [O II] doublet. The gratings, wavelength ranges, and central resolution values chosen for our program are shown in Table 1, for 2″ slit widths with a corresponding resolution element of 7.87 pixels. With two central wavelengths per grating, our program has a total of six spectroscopic settings that observe each mask. We will denote each dither as "Dither+" for the higher central wavelength and "Dither−" for the lower central wavelength. The astronomer's log recorded clear weather conditions during all observations for this mask. Seeing was 0.98″ for the PG3000 Dither−, 1.5″ for PG3000 Dither+, 1.1″ for PG2300 Dither−, 1.2″ for PG0900 Dither−, and 1.9″–2.4″ for PG0900 Dither+. For COSMOS-mask-B, the PG2300 Dither+ was not observed due to poor observing conditions. As a result, some chip gaps in this example have not been filled. However, the successful reduction of HETDEX J100041.45+021331.8 outlines the CARRSSPipeline's capabilities of reprojecting data even when settings are missing (see Section 4).

Table 1
Program Details

Grating	Camera Angles	$\lambda\lambda$	Central Resolutions
PG3000	76.75°, 70.00°	3409–4488 Å	$R \sim$ 1936, 2188
PG2300	70.75°, 66.25°	4197–5506 Å	$R \sim$ 1956, 2167[a]
PG0900	43.00°, 35.50°	5191–9530 Å	$R \sim$ 902, 1096

Notes. Observing techniques and details for our program that observed COSMOS-mask-B.
[a] Since PG2300 Dither+ was not observed in our COSMOS-mask-B, this value was measured using observations from another mask.

3. RSSMOSPipeline

We employ RSSMOSPipeline (Hilton et al. 2018) to carry out the preliminary reduction processes, which includes flat-field correction, cosmic ray rejection, sky subtraction, and wavelength calibration. Two of the main components of the package are the arc model generator and the reducer, which runs the scripts. RSSMOSPipeline performs these reductions on each spectroscopic setting separately, and outputs the 2D spectra as a Flexible Image Transport System (FITS) file. First, RSSMOSPipeline inspects the "product" folder (the outputted data files provided by the SALT-RSS PySalt package) and from there, performs gain correction, cross talk correction, and bias subtraction from these files. After, the three CCDs are then mosaicked together into a single image. Flat-fielding is then performed using the spectral flats we obtained from our observing scheme, where RSSMOSPipeline makes a spline fit to the flat field image in the dispersion axis. These reductions are done on the 2D spectra before extraction, then the images are rectified so the sky lines become vertical. This is useful because our wavelength calibrations are linear in individual settings, and each setting has its own arc model to perform

[11] https://github.com/GeorgeTheGeorgian/CARRSSPipeline.git
[12] https://RSSMOSPipeline.readthedocs.io
[13] https://github.com/saltastro/pysalt.git

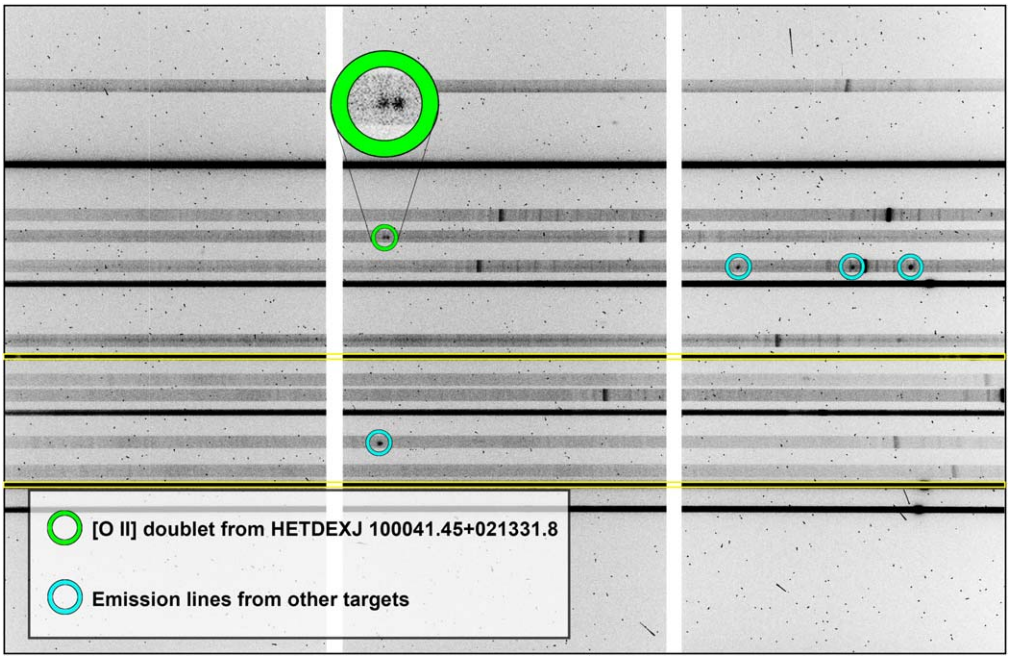


Figure 1. Science exposures of COSMOS-Mask-B taken with grating PG2300 at the lower central wavelength with some emission lines circled. Each horizontal slit is a separate target, and the fourth slit from the top with its [O II] doublet circled in green is J100041.45+021331.8, the HETDEX [O II]-emitter we follow throughout the paper. Lines from other targets, such as [O III] and Hβ, are circled in light blue. The six darkest spectra correspond to alignment star boxes, and slits 2 and 8 that are outlined in yellow are the SDSS stars that are used for flux calibration (see Section 4.1).

wavelength calibration. Since we seek to reproject the data onto a nonlinear wavelength array (see Section 4.2), it is useful for the wavelength calibration to be performed on each 2D setting prior to reprojection and 1D extraction.

While wavelength calibration is a standard procedure in spectroscopic reduction, our specific program requires reasonably accurate ($\sim$1 Å) wavelength agreement across multiple settings. The precision of this calibration influences subsequent steps, such as wavelength reprojection used for spectroscopic combination as detailed in Section 4.2. The output diagnostic plots from `RSSMOSPipeline` help the user visually inspect the wavelength solution and the features used to make them. The more features used from our model, the more accurate the wavelength solution. This can, however, become an issue when the arc image lacks noticeable features at low dispersion. Despite this, the wavelength solution shows that the centroid of the [O II] doublet from the PG2300 setting appears at $\lambda = 4938.9$ Å, which matches the HETDEX reported wavelength of $\lambda = 4938.38$ Å, to within an angstrom. We can further show the reliability of our wavelength solutions across other gratings by using the redshift calculated from the doublet and seeing if it is consistent with other lines. The results are consistent, with the redshift coming out to $z = 0.325$ for each line. Results for overall wavelength calibration accuracy are reported in Section 4.5.

4. CARRSSPipeline

We develop the `CARRSSPipeline`, a Python routine that compliments `RSSMOSPipeline`, to perform flux calibration, sky subtraction correction, wavelength reprojection, continuum comparison, and line inspection. This routine is designed to take several spectroscopic settings and combine them post calibration to cover a wavelength range of 3500–9500 Å and can be expanded or scaled down to accommodate as many settings as desired.

4.1. Flux Calibration

Flux calibration on SALT-RSS is considered highly challenging due to time variable primary mirror illumination resulting from the tracker moving as the sky rotates (Groenewald et al. 2023). However, we develop a novel approach for SALT-RSS by placing Sloan Digital Sky Survey (SDSS) stars as alignment stars on our slitmasks and using them as standards for flux calibration. Depending on the specific program and section of sky being observed, a user can include objects with flux calibrated spectra available from surveys other than SDSS, though we use SDSS due to its ubiquity and widespread presence. Kriek et al. (2015) followed a similar approach by placing secondary spectrophotometric standard stars on their Keck+MOSFIRE configurable slitmasks.

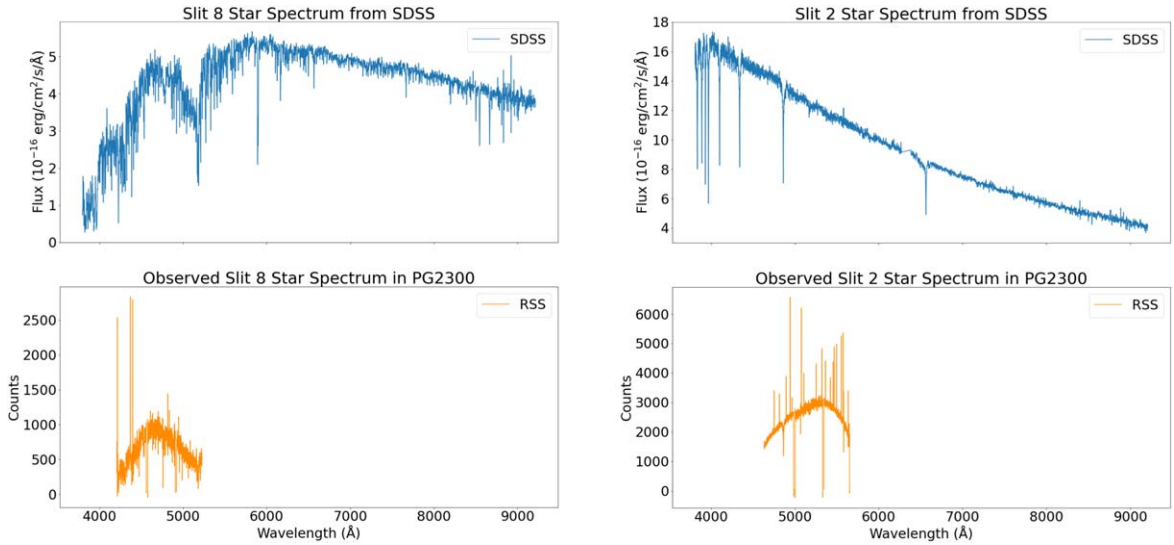


Figure 2. Plots for spectra from SDSS (upper/blue) and observed by RSS (lower/orange) of two alignment stars in COSMOS-mask-B. These are SDSS alignment stars in boxes and are visible in slits 2 and 8, which are highlighted yellow in Figure 1. This particular mask has only two reliable alignment stars with SDSS spectra, but the routine can accommodate an arbitrary number of stars. SDSS Slit 8 starts at around 4200 Å and SDSS Slit 2 ends at around 5650 Å, which is the range that the sensitivity function covers as shown in Figure 3.

Before flux calibration is carried out, `CARRSSPipeline` makes some adjustments to the RSS observed spectra. First, the pipeline sets all pixels making up chip gaps in observed RSS spectra to NaN; this helps with averaging since `RSSMOSPipeline` outputs them as zero, which can affect the average process for removing chip gaps and systematics. `RSSMOSPipeline` offers a sky subtraction routine that is designed for science slits, since science is not typically done on alignment stars. Due to the bright stars dominating the sky background in boxes that are 4″ on a side, `RSSMOSPipeline` over-subtracts "sky" on our observed SDSS star spectra, but we require accurate sky subtraction since they are used to flux calibrate our science spectra. That is why for each of the SDSS stars, `CARRSSPipeline` takes the top and bottom two rows of the spectrum and averages them to get an array of over-subtraction values for the top and bottom sides. Using those two average arrays, the pipeline makes a new array composed of their element-wise minima and re-subtracts the corresponding value from each column, bringing the edge values closer to zero and correcting for the missing flux. Choosing the smaller (more negative) value between the two average arrays for top and bottom regions makes the approach robust when a star spectrum is offset towards the top or bottom of the box, preventing the corresponding edge from representing the (over-subtracted) background level.

The routine makes a sensitivity function for each star by dividing the observed spectrum from SALT-RSS by the corresponding SDSS flux calibrated spectrum (see Figure 2). The resulting functions in units of counts/flux are then averaged together to form a combined sensitivity function. This combined sensitivity function is then smoothed to reduce the variance in the data, which is shown in Figure 3 for the PG2300 Dither− observation. This is done using a regression routine from the Python package `AstroML`[14] (Vanderplas et al. 2012), which outputs the second order polynomial coefficients for a smooth combined sensitivity function. We checked our internal consistency by running the `CARRSSPipeline` on the targets in this paper for each star individually and comparing fluxes between those spectra and the spectra reduced with both stars. The distribution of flux ratios show an average and median close to 1 as expected, and a scatter of 0.093 dex (24%) likely caused by errors in mask alignment and sky subtraction. We address this scatter by averaging the two stars before making a sensitivity function, and we suggest adding more than two stars in the observing masks to achieve higher precision, as it will further average out these variations from one star to another.

In addition, instances of wavelength mismatch between the observed RSS star spectrum and the corresponding SDSS star spectrum can negatively affect solutions due to extrapolation of data at the mismatch wavelengths. This occurs at the far blue and red ends in the PG3000 Dither− and PG0900 Dither+ settings, where our observed RSS star spectra wavelengths do not completely overlap with the wavelength range that SDSS has for their spectra.

To address this, we fit a polynomial to the sensitivity function using `SciPy`[15] (Virtanen et al. 2020) routines and the `AstroML` coefficients as initial guesses. This would just output an equivalent solution to `AstroML`, but we include an

[14] https://github.com/astroML/astroML.git
[15] https://github.com/scipy/scipy.git

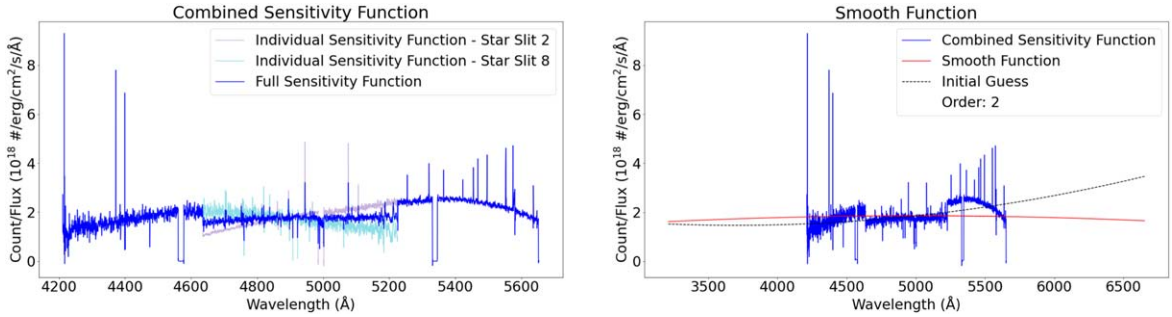


Figure 3. Plots showing diagnostic outputs from the `flux_calibration` function for the PG2300 Dither− observation. The left panel shows two individual sensitivity functions from each SDSS star, as well as their averaged combined sensitivity function in blue. Since the two stars have their maximum fluxes at different wavelengths, their average spectrum has an overlap region at roughly $\lambda\lambda = 4650$–5250 Å. This produces a rather anomalous combined sensitivity function, so we smooth it to bypass the jump discontinuities at the edges of the overlap region. The resulting smoothed function (solid red line) best represents the scale factor that should be applied to the science images.

additional constraint where the maximum value of this new function is set at a wavelength close to the maximum throughput of the setting. In the instance of wavelength mismatch, the initial guess and smooth function are no longer aligned, allowing the user to see how their custom polynomial compares to `AstroML` coefficients. In the instance of the PG2300 Dither− observation for HETDEX J100041.45 +021331.8, a maximum throughput constraint of 5000 Å was needed. This approach helps the user fit a polynomial when mismatch occurs, and is based on the specific spectroscopic setting used for the data.

After flux calibrating all settings for a particular target, we identified average offsets for wavelengths and fluxes of emission lines between overlapping settings. We additionally measure median continuum levels and compare those between settings (see Section 4.4 for details). Table 2 shows these values, where we see some deviation for wavelengths, line fluxes, and continuum fluxes between overlapping settings post flux calibration. The median deviation is 0.002 dex for line fluxes and −0.041 dex for continuum levels. The larger scatter seen for the continuum levels is expected because they are more sensitive to noise and wavelength mismatch than emission lines at specific wavelengths. Overall, we consider the overlapping data to be in good agreement.

Table 2
Statistical Comparison Throughout Reduction Processes

		$\Delta\lambda$ (Å)	[a]$\Delta(\log_{10} f)$ (dex)	[a]$\Delta(\log_{10} f_\lambda)$ (dex)
Overlapping	Mean	0.064	0.002	−0.131
	Median	−0.300	0.002	−0.041
	NMAD	1.038	0.044	0.128
Reprojected	Mean	0.150	−0.017	0.098
	Median	0.000	−0.004	−0.095
	NMAD	0.148	0.059	0.121

Notes. Comparing measurements of emission lines and continua between overlapping settings as well as before and after reprojection for observed RSS science spectra. f denotes fluxes of emission lines and f_λ denotes median flux levels of continua. For comparisons between overlapping settings, negative values mean higher values for the bluer of the two settings. For comparisons before and after reprojection, negative values mean higher values for the combined reprojected spectrum. To convert to percent error, use % Error $= (10^{\Delta(\log_{10} F)} - 1) \times 100$.
[a] Calculated using formula: $\Delta(\log_{10} F) = \log_{10}(F_a/F_b)$, where F_a, F_b are corresponding fluxes for spectra a, b.

4.1.1. Slit Losses

Alignment stars on RSS are typically put in $4'' \times 4''$ boxes. Compared to $2'' \times 10''$ science slits, the greater box width allows more of the starlight to be observed and helps with mask alignment. Since the `CARRSSPipeline` uses the flux density of SDSS stars to flux-calibrate the science spectra, the greater (horizontal) slit losses for science targets contribute to a multiplicative bias (see Section 4.3 for details on how the bias for this mask was derived and the procedure to correct it). To reduce this multiplicative bias and simplify the analysis, in the future we suggest putting spectrophotometric alignment stars in slits the same size as the science slits, as this should match the slit losses from science targets. This is similar to how Kriek et al. (2015) conducted flux calibration for the MOSFIRE instrument on the Keck I telescope, which utilizes a cryogenic configurable slit unit (CSU) that allows them to change a star box into a star slit after mask alignment. One drawback for SALT-RSS is that slits are not configurational, so putting a bright SDSS star in a slit means we lose a star for mask alignment.

Our science targets are placed in $2'' \times 10''$ slits, which as noted above are more susceptible to slit losses, especially if the object is

Table 3
PSF Gaussian Fractional Slit Loss

Seeing/FWHM	Point Source	Extended Source
1.0″	0.017	0.351
1.4″	0.089	0.384
1.8″	0.186	0.421
2.0″	0.234	0.440
2.4″	0.321	0.476

Note. Estimates of slit losses for 2″ × 10″ slits, measured by creating an isotropic 2D Gaussian PSF on our science slits for both point sources and extended objects. Seeing values were obtained from observing logs for COSMOS-mask-B.

extended like many of our HETDEX targets. Slit losses affecting our science observations are due to a combination of PSF width, astrometric errors in mask design, and imperfect mask alignment; hence our procedures to correct for them will not be perfect. Table 3 shows our rough estimates for slit losses, derived from applying a normalized 2D Gaussian PSF over the slit. For the extended HETDEX targets in this paper, the extended source values are expected to better predict the multiplicative bias between flux calibration from the SDSS stars and our eventual cross-check versus emission line fluxes in the HETDEX catalog.

4.2. Full-Optical Spectroscopic Combination

Figure 4 shows HETDEX J100041.45+021331.8 in all Dither− settings after it has been run through the `RSSMOSPipeline`, but prior to the `CARRSSPipeline`. The [O II] doublet is visible in PG2300 and is resolved due to high SALT-RSS resolution. We can also see Hβ and [O III]λ4959,5007 in PG0900. Following flux calibration of the data, these spectroscopic settings, along with their Dither+ counterparts, are combined on a single projected "wavelength" axis yielding a fully reprojected, flux-calibrated, 2D spectroscopic image of the target. The settings are reprojected onto an exponential function of wavelength, and we intentionally over-sample in the PG0900 settings to maintain (nearly) full resolution in the PG3000 and PG2300 settings.

$$\lambda = A\left(\exp\left(\frac{L}{k}\right) + D\right) \tag{1}$$

$$\Delta\lambda = \frac{d\lambda}{dL} = \frac{A}{k}\cdot\exp\left(\frac{L}{k}\right) \tag{2}$$

$$R(L) = k\left(1 + D\ \cdot\ \exp\left(-\frac{L}{k}\right)\right) \tag{3}$$

Equation (1) shows the exponential function used in our reprojection, where L is a linear array of values that takes the place of a traditional wavelength array, k determines the asympototic resolution at long wavelengths, A is a scaling factor that causes the reprojected array to begin at the desired wavelength, and D determines the fractional drop in resolution from the first pixel to its asymptotic value. Equation (2) gives us $\Delta\lambda$ by taking the derivative of λ with respect to L. Dividing Equations (2) from (1) gives us our resolution function in Equation (3). When $L = 0$, $R = k(1+D)$; as $L \rightarrow \infty$, $R = k$. Therefore the resolution from $L = 0$ to ∞ drops by kD, and we pick $D = 1$ to achieve our desired factor of 2 drop from the start to the asymptotic value. One can also choose D by defining R_0 and R_∞ and using $D = (R_0 - R_\infty)/R_\infty$. Then the parameter A can be chosen based on the starting wavelength, $A = \lambda_{\rm start}/(D+1)$. Note that here, $\lambda_{\rm start}$ corresponds to $L = 0$.

Figure 5 illustrates the resolution versus wavelength of the reprojected axis as well as the oversampling of the PG0900 settings. A potential limitation arises when data are present at overlapping wavelengths in both the PG2300 and PG0900 settings; since the resolution per pixel in the PG0900 settings is much lower than the PG3000 and PG2300 counterparts, features such as [O II] doublets lose resolution post reprojection. To prevent this, the `CARRSSPipeline` has a minimum resolution threshold that favors higher resolution settings. If there are two settings at a given wavelength above or below the threshold, they get averaged normally, otherwise if there is one below the threshold and one above the threshold, it will use the higher resolution setting. With this parameter, [O II] doublets retain their resolution as seen in Figures 6 and 7. After reprojecting all settings for a particular target on a common exponential wavelength axis, we identified average offsets for wavelengths and fluxes of emission lines between individual spectra and the reprojected spectrum. We also measured median continuum levels and compared those between individual spectra and the reprojected spectrum (see Section 4.4 for details). Table 2 shows these values, with good agreement of −0.004 dex for line fluxes and decent agreement of −0.095 dex for continua.

4.3. 1D Extraction

After the `CARRSSPipeline` outputs a fully combined flux-calibrated 2D spectrum, the target signal is extracted and saved as a 1D spectrum. We utilize the `finalExtration` function on `RSSMOSPipeline` to obtain trace centers and sigmas for each column, with a moving window of several hundred pixels. The trace centers and sigmas generate Gaussian fits across the spatial axis of the 2D RSS science spectra. We checked to see if the spatial profiles can be represented well as Gaussian for both the science spectra and the star spectra, and found that they do appear Gaussian and have FWHM values comparable to the seeing values outlined in Section 2. The `finalExtration` function also offers a linear running profile made using the trace centers and sigmas, but we instead implemented a custom trace fitter in the `CARRSSPipeline`

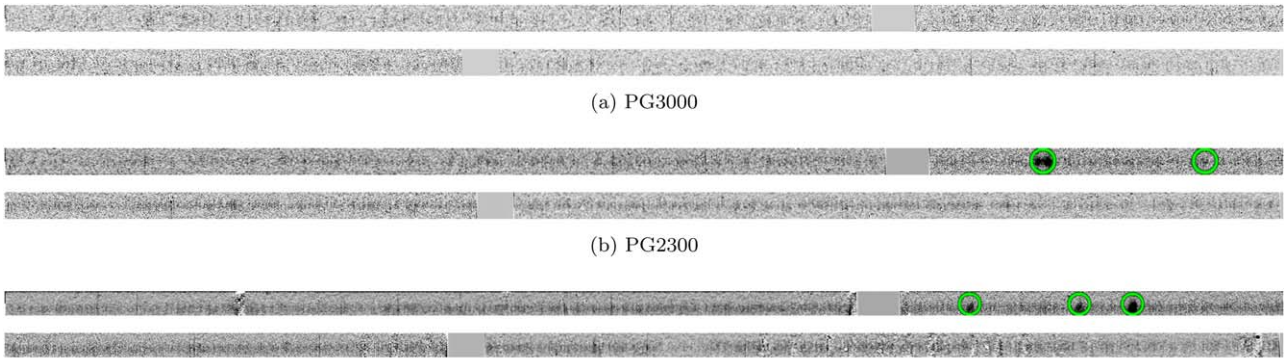


Figure 4. Above are 2D spectroscopic images of HETDEX J100041.45+021331.8 post `RSSMOSPipeline` calibration, but prior to `CARRSSPipeline` in all Dither− gratings. [O II] and [Ne III] λ3869 are visible in PG2300 Dither−, while [O III] λ4959,5007 and Hβ are visible in PG0900 Dither−.

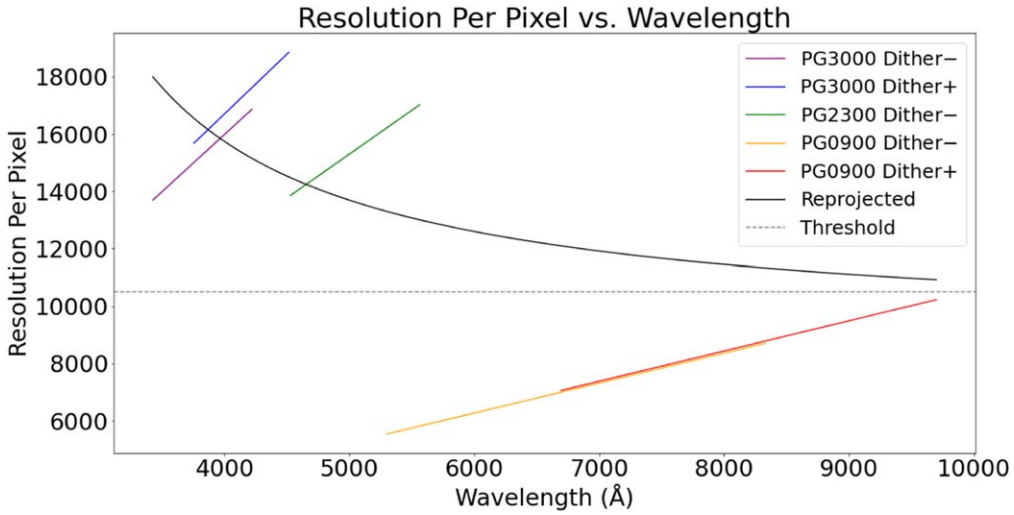


Figure 5. Resolution plot showing the relationship between resolution per pixel and wavelength. The colored lines represent each setting, with the color corresponding to the grating (violet/blue for PG3000, green for PG2300, orange/red for PG0900) and the sign representing the grating angle (Dither+ for the upper angle and Dither − for the lower angle). The solid black line is the reprojected wavelength axis that the routine generates using an exponential fit. The dashed gray line is the minimum resolution threshold parameter used to favor higher resolution settings when they overlap with others.

that makes a running profile using a polynomial fit of order 4. Finally, we multiply the 2D RSS science spectra with this profile and sum the weighted rows to extract the 1D spectrum. Figure 8 shows the `CARRSSPipeline` outputted 1D spectrum for HETDEX J100041.45+021331.8 spanning the full wavelength coverage. The pipeline allows the user to select which settings they want to include given the context of their specific program.

Table 4 shows how the flux calibration of RSS observed science spectra compares to that of HETDEX for emission lines fluxes (f) and median flux values of the fitted continuum (f_λ) across the wavelength range that overlaps with HETDEX coverage (see Section 4.4 for details on continua measurements). These values were derived by comparing line fluxes of six emission lines and continuum levels of their host galaxies to their published HETDEX catalog values, as can be seen in Section 4.5. The offsets are essentially an average of offsets from multiple settings that have been reprojected and averaged together over the exponential wavelength array from earlier. Since Table 2 shows that flux calibrations of individual settings agree well with each other and with the reprojections, a single averaged offset can be used as a multiplicative bias. These measurements indicate that the multiplicative bias for this mask in reference to HETDEX is −0.286 dex. We attribute this factor of ∼2 flux loss to a combination of astrometric errors affecting mask design, imperfect mask alignment, and atmospheric seeing. This factor matches well with our slit loss estimates for extended objects shown in Table 3, supporting the idea that these slit losses are the key contributor to

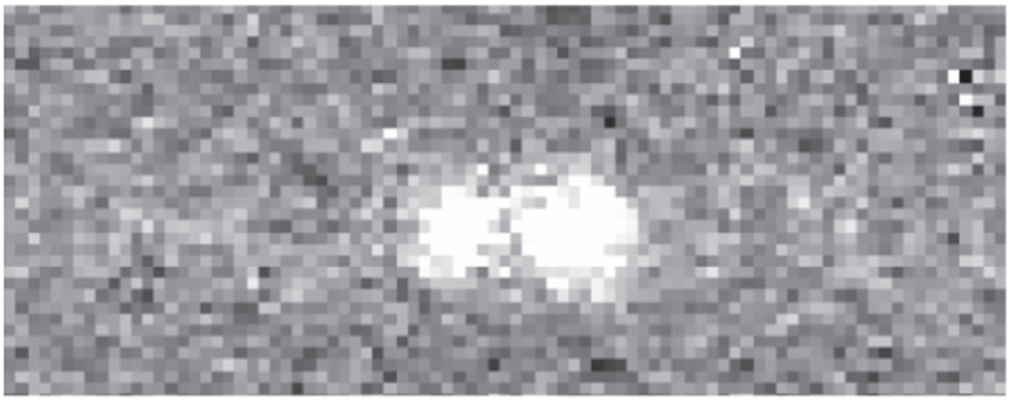


Figure 6. The [O II] doublet from HETDEX J100041.45+021331.8 after it has been flux calibrated and reprojected. The resolution of the [O II] doublet is well preserved.

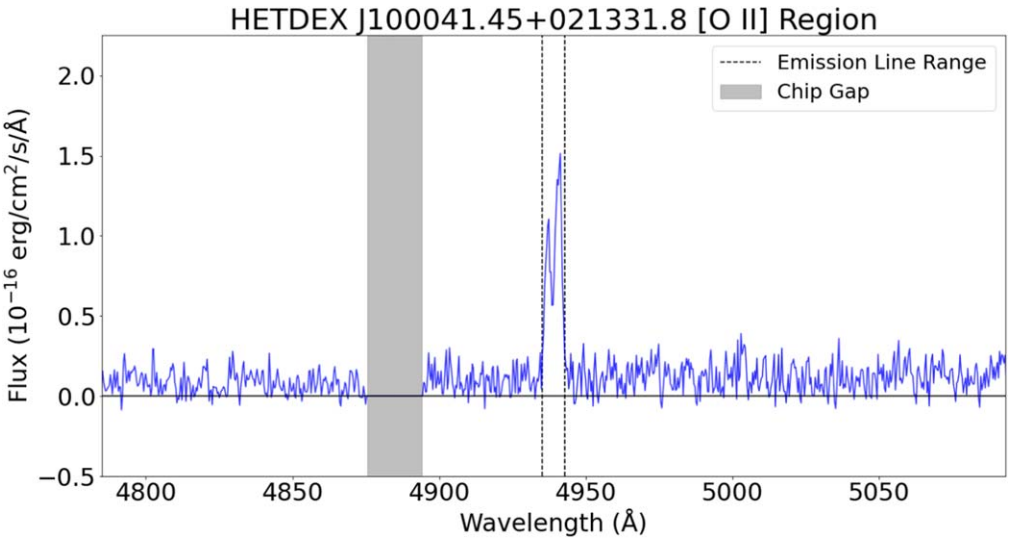


Figure 7. The [O II] doublet from HETDEX J100041.45+021331.8 in the reprojected spectrum at $\lambda = 4938.38$ Å.

this multiplicative bias. All flux data reported in subsequent tables and flux-calibrated spectra shown in figures in this paper have already been corrected for this bias, which we implement in the `CARRSSPipeline` as the multiplicative bias parameter. The pipeline defaults this value to one unless the user can identify their own offset dependent on their specific program, which could be done by including flux-calibrated targets from the literature and comparing to the `CARRSSPipeline`'s calibration. If such an offset is identified, the `CARRSSPipeline` should then be run a second time with the multiplicative bias parameter set to this value.

4.4. Continuum Comparison

If the observed source has an available spectrum in the literature to compare with, the user can take advantage of the spectral comparison function `continuum_comparison` offered by the `CARRSSPipeline`. In addition to comparing continua, it also plots the extracted signal for each setting and for the combined setting, all post flux calibration. This allows the user to visually compare the continua of reduced spectra against literature spectra across the same wavelength range. Figure 9 shows these outputs for HETDEX J100041.45 +021331.8, where we can further confirm the wavelength calibration accuracy by seeing the [O II] doublets overlapped. These continuum comparisons have been carried out for all targets in this paper, and those results are shown in Table 5. The larger disagreement for HETDEX J100057.95+021524.4 comes from the bluest observation, where the flux calibration was significantly affected by poor data quality at low wavelengths. Overall, the median continuum values between

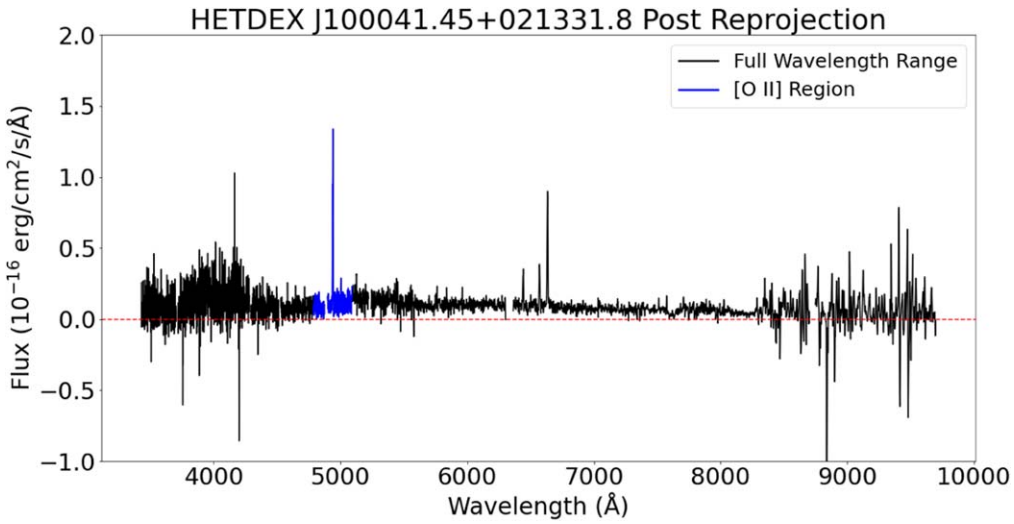


Figure 8. This plot illustrates the 1D flux calibrated, reprojected spectrum of HETDEX J100041.45+021331.8 after Gaussian smoothing with a sigma = 1.5 pixel kernel. The bluest setting is noisy but the continuum level still matches HETDEX relatively well. The [O II] region shown in Figure 7 is highlighted in blue.

Table 4
Flux Statistics Between RSS and HETDEX Spectra

	[a]$\Delta(\log_{10} f)$ (dex)	[a]$\Delta(\log_{10} f_\lambda)$ (dex)
Mean	−0.292	−0.367
Median	−0.286	−0.358
NMAD	0.064	0.141

Notes. Comparing statistical offsets of emission lines and continua between our observed RSS science spectra and HETDEX. f denotes fluxes of emission lines and f_λ denotes median flux levels of continua. Positive values denote overestimation and negative values denote underestimation compared to HETDEX.
[a] $\Delta(\log_{10} F) = \log_{10}(F_{\rm rss}/F_{\rm hetdex})$.

Table 5
Flux Measurements for Continua

Target Name	[a]$f_{\lambda,\rm rss}$	[b]$\Delta(\log_{10} f_\lambda)$ (dex)
HETDEX J100057.95+021524.4	0.025	−0.512
HETDEX J100048.38+021454.2	0.361	0.023
HETDEX J100032.77+021357.3	0.229	−0.128
HETDEX J100041.45+021331.8	0.133	0.060

Notes. Fluxes here denote median values of the fitted continuum across the wavelength range that overlaps with HETDEX coverage. Positive (negative) values in the final column denote overestimation (underestimation).
[a] In units of 10^{-16} erg cm^{-2} s^{-1}.
[b] Calculated using formula: $\Delta(\log_{10} f_\lambda) = \log_{10}(f_{\lambda,\rm rss}/f_{\lambda,\rm hetdex})$.

our RSS observed spectra and HETDEX agree to an average of −0.14 dex.

4.5. Line Visual Inspection

All targets in this paper have been observed by HETDEX, allowing us to compare line fluxes and wavelengths for [O II] doublets and other available lines. The `CARRSSPipeline` offers a function called `line_inspection` that takes in the emission line wavelength range and a configuration file with known emission line rest wavelengths. Using these, the centroid of the emission line is calculated using the centroid function offered by another Python package called `Specutils`[16] (Earl et al. 2024), and used to measure the observed wavelength and redshift of our RSS observed science spectra. Before line flux measurements are carried out, the spectra are first subject to continuum subtraction, which takes advantage of a continuum fitter from `Specutils`. The `line_inspection` function also uses the `line_flux` function from `Specutils`, which takes the integrated flux of the emission line over the emission line wavelength range and outputs both the line flux and an error that is based on an empirical method of fitting the spectrum to a polynomial and measuring the root mean squared of the signal at each point. A limitation of this approach arises due to systematics that causes spikes by poorly subtracted sky lines, but we manage this limitation by using a moving window of 100 pixels to measure the RMS at each pixel. Figure 7 shows a 1D extraction of the [O II] doublet from HETDEX J100041.45+021331.8 made from this module. Table 6 shows the emission line wavelength and line flux

[16] https://specutils.readthedocs.io/en/stable/

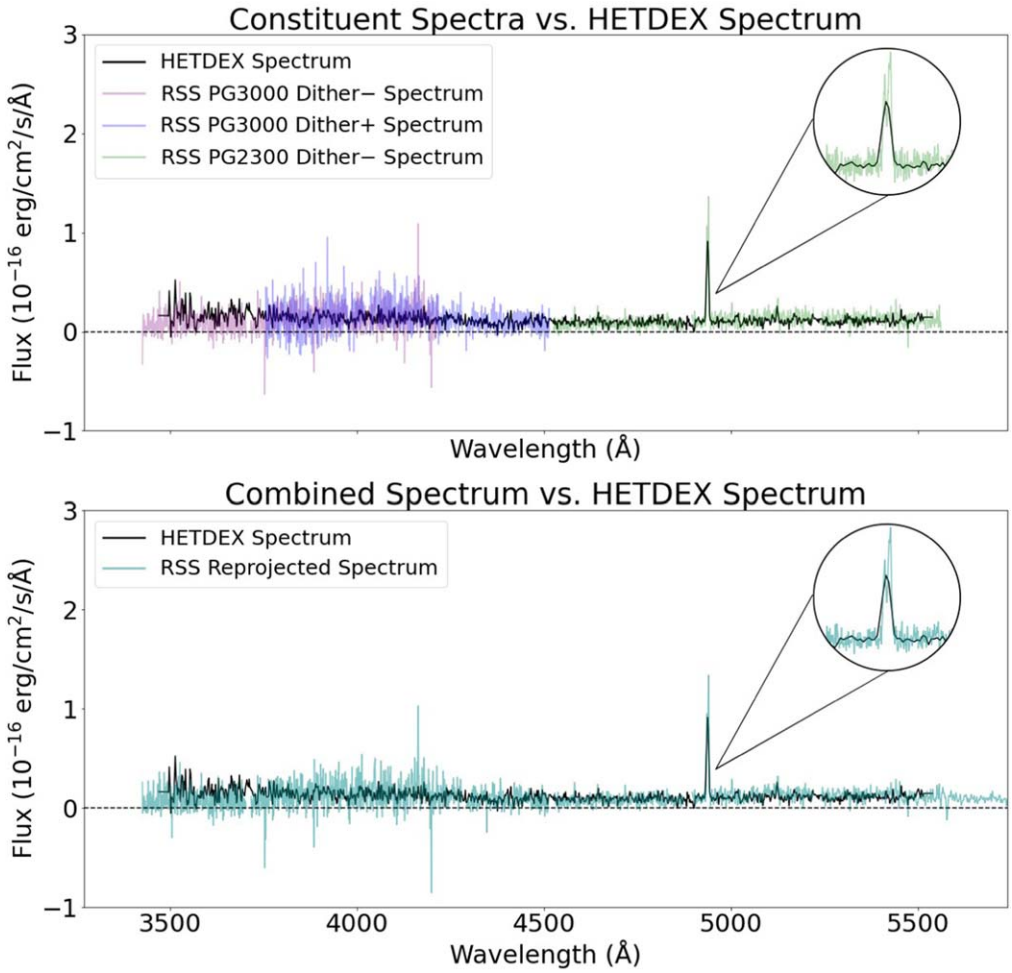


Figure 9. Plots outputted from the spectral comparison function showing all the extracted signals of spectra from each setting (upper plot) and the combined spectrum (lower plot) compared to the HETDEX spectrum for J100041.45+021331.8 after Gaussian smoothing with a sigma = 1.5 pixel kernel. Note that the [O II] doublets overlap but is unresolved in the HETDEX spectrum ($R \sim 800$).

Table 6
Wavelength and Flux Measurements for Emission Lines

Target Name	Line	Confidence	λ_{rss} (Å)	[a] σ_λ (Å)	z	Δz	[b] f_{rss}	[b] σ_f	[c] $\Delta(\log_{10} f)$ (dex)
HETDEX J100057.95+021524.4	[O II]	2	5030.3	1.7	1.34954	0.00062	3.172	0.203	−0.118
HETDEX J100048.38+021454.2	[O II]	3	4074.0	0.8	1.09297	0.00017	7.276	0.195	0.049
HETDEX J100048.38+021454.2	Hβ	3	5313.1	0.4	1.09293	0.00013	1.997	0.056	−0.063
HETDEX J100048.38+021454.2	[O III]λ5007	2	5471.3	0.5	1.09277	−0.00003	1.436	0.064	0.011
HETDEX J100032.77+021357.3	[O II]	3	4184.9	1.3	1.12273	0.00064	9.771	0.138	−0.061
HETDEX J100041.45+021331.8	[O II]	3	4938.9	1.6	1.32500	0.00086	5.882	0.153	0.014

Notes. Confidence denotes how visible the emission line is in both the 2D and 1D spectra. 3 is completely visible and distinct from surrounding noise; many with confidence 3 are visible before reduction even begins. 2 is clearly visible, slightly noisier and may appear less Gaussian. These may be hard to see prior to reduction. 1 denotes that something is there, but difficult to see even after reduction. Positive values denote overestimation and negative values denote underestimation compared to HETDEX.

[a] Median offsets outputted by `RSSMOSPipeline` by comparing the wavelength solutions to a dictionary of sky lines.

[b] In units of 10^{-16} erg cm^{-2} s^{-1}.

[c] Calculated using formula: $\Delta(\log_{10} f) = \log_{10}(f_{rss}/f_{hetdex})$.

measurements for each target. Wavelength calibrations for all targets in this paper are good to within $\sim \pm 300\,\mathrm{km\,s^{-1}}$ ($\Delta z = 0.001$), with most being good to $\sim \pm 30\,\mathrm{km\,s^{-1}}$ ($\Delta z = 0.0001$).

5. Conclusions

With the goal of expanding the scientific capabilities of SALT-RSS, our `CARRSSPipeline` is designed to minimize a physical limitation that arises from the variable primary mirror illumination seen by the tracker. By using SDSS stars with calibrated spectra as alignment stars, our program allows astronomers to perform a rough flux calibration of science spectra. The pipeline follows with reprojection and 1D extraction routines that output fully reprojected science spectra ready for line flux and continuum analysis that the `CARRSSPipeline` also offers.

The pipeline is sensitive to RSS observed star spectra quality. Our COSMOS-mask-B observed alignment stars in square boxes as opposed to science slits. As a result, our analysis of flux calibration required a two-step process where we first used the SDSS box stars to perform relative flux calibration, then used known HETDEX flux measurements to measure a multiplicative bias. Removing this multiplicative bias achieved a rough flux calibration. Since most multi-slit spectroscopy observations do not include targets with known emission-line fluxes, we suggest matching the slit losses by putting SDSS stars in slits the same size as the science slits. The median line flux error of −0.286 dex seen in Table 4 represents a multiplicative bias for our program, which we then correct for during flux calibration. This bias matches our estimates of slit losses for extended objects seen in Table 3 for various seeing values obtained during observations. All flux data reported in this paper have already been corrected for this bias, as well as all figures that show flux-calibrated spectra. After correcting for this bias, the `CARRSSPipeline` achieved a 0.064 dex accuracy for these targets as reflected by the normalized median absolute deviation, meaning that the pipeline can be capable of rough flux calibration close to 20% especially if calibration objects are placed in slits the same size as the science slits. We expected this value to be less than the 0.093 dex scatter between two stars from the independent cross-check from Section 4.1, since the goal of averaging them is to reduce these calibration uncertainties.

After reducing all observational data, analyses of emission lines will shed light on various galaxy characteristics for these [O II]-emitters. A follow-up paper detailing flux analyses and science will follow the reduction of all masks at our disposal, giving us an improved view of [O II]-emitting galaxies.

Acknowledgments

We would like to thank the Department of Physics & Astronomy at Rutgers University, SALT staff, and collaborators from ODIN for their support. We acknowledge support from NSF grants AST-2206222 and AST-2206705, as well as NASA Astrophysics Data Analysis Program grant 80NSSC22K0487. EG acknowledges the support of an IBM Einstein fellowship for his sabbatical at IAS during the completion of this manuscript.

This material is based upon work supported by the National Science Foundation Graduate Research Fellowship Program under grant No. DGE-2233066 to NF. N.F. would also like to thank the LSST-DA Data Science Fellowship Program, which is funded by LSST Discovery Alliance, NSF Cybertraining grant 1829740, the Brinson Foundation, and the Moore Foundation; her participation in this program has benefited this work.

Facility: SALT.

Software: `Astropy` (Robitaille et al. 2013, Price-Whelan et al. 2018, Astropy Collaboration et al. 2022), `AstroML` (Vanderplas et al. 2012), Principal Investigator Proposal Tool (PIPT), `PySALT` (Crawford et al. 2010), `RSSMOSPipeline` (Hilton et al. 2018), `SciPy` (Virtanen et al. 2020), `Specutils` (Earl et al. 2024).

ORCID iDs

George V. Kharchilava https://orcid.org/0000-0002-0927-7554
Eric Gawiser https://orcid.org/0000-0003-1530-8713
Matt Hilton https://orcid.org/0000-0002-8490-8117
Nicole M. Firestone https://orcid.org/0000-0002-9811-2443
Kyoung-Soo Lee https://orcid.org/0000-0003-3004-9596

References

Astropy Collaboration, Price-Whelan, A. M., Lim, P. L., et al. 2022, ApJ, 935, 167
Crawford, S. M., Still, M., Schellart, P., et al. 2010, Proc. SPIE, 7737, 773725
Earl, N., Tollerud, E., O'Steen, R., et al., 2024 astropy/specutils: v1.19.0, zenodo:10.5281/zenodo.1421356
Gebhardt, K., Mentuch Cooper, E., Ciardullo, R., et al. 2021, ApJ, 923, 217
Groenewald, D., Hettlage, C., Kniazev, A., et al. 2023, https://pysalt.salt.ac.za/proposal_calls/current/ProposalCall.html
Hill, G. J., Lee, H., MacQueen, P. J., et al. 2021, AJ, 162, 298
Hilton, M., Hasselfield, M., Sifón, C., et al. 2018, ApJS, 235, 20
Kriek, M., Shapley, A. E., Reddy, N. A., et al. 2015, ApJS, 218, 15
Piskunov, N., Wehrhahn, A., & Marquart, T. 2021, A&A, 646, A32
Price-Whelan, A. M., Hogg, D. W., Rix, H. W., et al. 2018, ApJ, 156, 18
Prochaska, J. X., Hennawi, J. F., Westfall, K. B., et al. 2020, JOSS, 5, 2308
Prochaska, J. X., Hennawi, J., Cooke, R., et al., 2025 pypeit/PypeIt: Release v1.17.2, zenodo:10.5281/zenodo.3506872
Ramsey, L. W., Adams, M. T., Barnes, T. G., et al. 1998, Proc. SPIE, 3352, 34
Robitaille, T. P., Tollerud, E. J., Greenfield, P., et al. 2013, A&A, 558, A33
Vanderplas, J., Connolly, A., Ivezić, Ž., & Gray, A. 2012, Introduction to astroML: Machine learning for astrophysics, in Conf. on Intelligent Data Understanding (CIDU) 24-26 October 2012 (Boulder, CO, USA: IEEE), 47
Virtanen, P., Gommers, R., Oliphant, T. E., et al. 2020, NatMe, 17, 261